Low velocity impact on crash components with steel skins and polymer foam cores

Aase Reyes , Tore Børvik

PII: S0734-743X(18)31039-X
DOI: https://doi.org/10.1016/j.ijimpeng.2019.05.011
Reference: IE 3297

To appear in: *International Journal of Impact Engineering*

Received date: 15 October 2018
Revised date: 6 May 2019
Accepted date: 9 May 2019

Please cite this article as: Aase Reyes , Tore Børvik , Low velocity impact on crash components with steel skins and polymer foam cores, *International Journal of Impact Engineering* (2019), doi: https://doi.org/10.1016/j.ijimpeng.2019.05.011

Highlights:

- The mechanical properties of XPS and EPP depend strongly on the foam density
- XPS and EPP are found to be strain-rate sensitive even at low strain rates
- XPS absorbs more energy than EPP in quasi-static indentation tests
- The core material is found to be of less importance in dynamic tests
- The foam density in an efficient energy absorber should be as low as possible

Low velocity impact on crash components with steel skins and polymer foam cores

Aase Reyes[a,b,*] and Tore Børvik[a,b]

[a] *Structural Impact Laboratory (SIMLab), Department of Structural Engineering, Norwegian University of Science and Technology (NTNU), NO-7491 Trondheim, Norway*

[b] *Centre for Advanced Structural Analysis (CASA), NTNU, NO-7491 Trondheim, Norway*

Abstract

Energy absorbing systems are extensively used in the automotive industry to ensure crashworthiness. Such crash components could typically consist of a sandwich structure with thin ductile plates as skins and a cellular foam as core to dissipate the kinetic energy. In a previous study, the quasi-static behaviour of two polymeric foam types with different densities, namely extruded polystyrene (XPS) and expanded polypropylene (EPP), used as core material in typical crash components was examined. The investigation involved a large number of compression tests of the core materials loaded in different material directions and indentation tests on sandwich structures in different configurations. In the present study, low-velocity impact tests are conducted in a drop tower on the same target configurations consisting of 0.8 mm thick skins of Docol 600DL steel and the various foams as core. During testing, the dropped mass was kept constant at approximately 15 kg, while the impact velocity varied between 5 and 10 m/s. The impact force was registered by the instrumented striker of the drop tower, and these measurements were used to obtain the displacement of the striker and the energy absorption of the different crash components. In addition, high-speed cameras and 3D-DIC were used to measure the out-of-plane displacement of the back skin. The presented results indicate that to minimise the weight and at the same time maximize the energy absorption of the crash component, a low density foam should be used as core material. It is also shown that by proper design, it is possible to optimize the protection level of such components, at least within a given velocity range.

Keywords: Sandwich structures; Material tests; Impact tests; Energy absorption

1. Introduction

In the automotive industry, energy-absorbing systems have become ever more important to ensure protection of the car body and the passengers during a crash event [1]. In the pursuit

* Corresponding author.

e-mail address: aase.reyes@ntnu.no (A. Reyes)

of new innovative designs and materials, often driven by the prospect of weight reduction, research in this field is evolving rapidly [2]. Among such energy-absorbing systems are crash pads located inside the vehicle to improve the passengers' survivability, special designs for pedestrian safety, and bumper-beam systems with crash boxes for increased crashworthiness. A sandwich structure with a core material inserted between two skins could be part of such a system. Here, the core is typically a light and soft cellular foam that absorbs energy by crushing. Foams are also found inside other structural elements for passive safety in a car body [3], and sometimes foams are intended to absorb energy without any outer skin or casing [4]. In either case, many factors need to be considered in the design of an energy absorber. The dissipation should be as high as possible, which can be achieved through high forces or large displacements of the component, but the transferred loads should not be too high for both passenger safety and structural integrity. In addition, there might be limitations on the maximum displacement of the crash component. It would be favourable if the load can be kept constant at a low level, while at the same time absorb considerable amounts of energy through crushing of the component.

Cellular materials such as honeycombs and foams have excellent characteristics as energy absorbers due to their ability to deform over a long stroke at an almost constant load [5]. The characteristics of these materials are governed by the topology of the cell structure and the intrinsic properties of the cell-wall material, where the topology defines how the constituent material is packed in space to form a porous structure. While honeycombs have a periodic topology, foams are in general stochastic. Polymeric foams have been particularly attractive because of their low weight, excellent energy absorbing capability, insulation properties, easy production, low price and design flexibility. Nowadays, they are used in many applications, such as protective materials including packaging and head protective systems, and in a multitude of aerospace, marine and automotive components [6]-[8]. A large number of polymeric foams are available, and their microstructures depend on the base material and the production process that influence the density as well as the thermal and mechanical properties.

Foams are generally classified into open or closed cell foams. Despite the many variations, the typical mechanical compressive response of most polymeric foams contains three phases of deformation [9]. The first phase is the linear elastic region that is governed by the reversible bending or distortion of the cell walls during small deformations [10]. The second phase is the plateau region with large deformations that occur at modestly increasing stress levels and is primarily related to buckling of the cell walls. This phase is the attractive

feature for energy absorption, i.e., the ability to withstand large deformations at an approximately constant stress level. The third phase is the densification region that begins when the cell walls interact with each other, even before all voids have collapsed, and this causes the stress to rise rapidly. Theoretically, the densification strain is defined as when zero void ratio is reached [10]. However, the meaning of this term varies in the literature and is sometimes taken as the strain at the onset of the densification region, i.e., when the cell walls start to interact with each other [11]. Important properties of foams include low relative density (< 0.3) and high specific energy absorption, where the absorbed energy per unit volume is approximated by the area beneath the stress-strain curve [9]. In general, the mechanical properties of foams have been found to depend strongly on the density; e.g. the elastic modulus and plateau stress will increase, while the densification strain will decrease, with increasing density [9][12]. The constitutive behaviour of most polymeric foams is both strain-rate and temperature dependent [13], and a comprehensive review on the dynamic compressive behaviour of cellular materials was recently published by Sun and Li [14]. Another feature that has received some attention lately is the anisotropic behaviour of polymeric foams [15][16]. Although the structural anisotropy is believed important in order to tailor the mechanical properties of foams, few investigations have analysed this in any detail.

A sandwich panel used for energy absorption typically consists of two sheets attached to a deformable core [17]. The idea is that the core will absorb energy during the impact event, and as a result, lower the impulse transferred to the surrounding structure. A distinction is often made between a sacrificial cladding (i.e., a sandwich panel that is fixed to an existing structure) and a sandwich structure where the rear side is free to deform [18]. The application usually governs the choice of skin and core material. Aluminium [19][20], steel [21][22], and glass-fibre-reinforced polymer (GFRP) [23][24] sheets have all been used in combination with various cores. Some authors have tried to investigate the influence of the foam core density in a systematic manner [25][26], while others have played with the idea of designing foam components with graded density according to where compressive strength is needed [27]-[29]. These studies have shown that the core material and density are important design parameters, and that the performance can be optimized with a proper choice of material. They also show that it is not straightforward to optimize such components experimentally, and that both extended experimental databases and accurate material models for numerical simulation are needed to improve the optimization process.

From the literature, it is clear that a myriad of different foam and skin materials that can be combined to create a sandwich panel exist. In the present experimental investigation, we

wanted to reveal the energy absorbing capability of two different polymeric foams (XPS and EPP) used as core material in a crash component in a systematic manner. XPS is mainly used as an insulation material, while EPP is typically applied for energy absorption. Both the base material and the production method differ significantly between the two foams. Three different densities have been tested for each foam type. To characterize the foams, a large number of compression tests were conducted on specimens loaded in different material directions at both quasi-static and elevated strain rates. Then, quasi-static and dynamic impact tests on sandwich structures were performed. While the quasi-static tests have been reported in a recent publication by Reyes and Børvik [30], this paper focuses on the dynamic response of the same materials and components. The sandwich panels applied in the dynamic impact tests consisted of 50 mm thick polymeric foam cores and skins of 0.8 mm thick Docol 600DL steel plates. Components without the front skin were also tested to investigate the effect of covering the core. The tests were conducted in a drop tower with a constant mass of about 15 kg, while the impact velocity was varied between 5 and 10 m/s. The impact force was registered by the instrumented striker of the drop tower, while high-speed cameras and 3D-DIC were used to measure the out-of-plane displacement of the back skin. Within the experimental limitations of this study, it seems clear that in order to minimise the weight and at the same time maximize the energy absorption of the crash component, a low-density foam should be used as core material. We also found that the energy absorption and the back-skin displacement during crushing depend on the impact velocity range, in addition to the core material and density.

2. Materials

2.1 Skin and core materials

The skins of the crash components are made of 0.8 mm thick plates of the dual-phase steel Docol 600DL. This material is frequently used in car safety components, and the plates were produced and delivered by Swedish Steel AB (SSAB). Nominal values for the yield stress is between 280 and 360 MPa, while the tensile strength varies between 600 and 700 MPa. Due to the nominal density of steel, it cannot be defined as a lightweight material, and the areal weight of the crash components could have been significantly reduced by selecting a lighter material. However, we decided to use Docol 600DL to avoid fracture in the component during impact as both its strength and ductility are high compared to most light alloys.

Two types of polymeric foam with a nominal thickness of 50 mm and three different densities are considered as core material. The first foam is extruded polystyrene (XPS) from Sundolitt [31]. XPS is a closed-cell foam based on the monomer styrene having a typical density range of about 28-45 kg/m^3, high relative strength, low thermal conductivity, and is mainly utilized as thermal insulation. Continuous foam plates are produced by an extrusion process where molten beads of polystyrene is mixed with a blowing agent and other additives before it is extruded through a flat nozzle, which gives the plates their desired profile and thickness. Three different nominal densities of XPS have been investigated here, namely 30, 35 and 45 kg/m^3, called XPS-250, XPS-400 and XPS-700, respectively. The digits in the names indicate the plateau stress of the material in kPa. The XPS foams were delivered as plates with nominal dimensions 1185 mm × 585 mm × 50 mm. The second core material is expanded polypropylene (EPP) from ARPRO [32]. EPP is an addition thermoplastic polymer made from the monomer propylene with a density range from 20 to 200 kg/m^3. EPP has many of the same beneficial properties as XPS, but in contrast to XPS, which is rather friable and may break upon impact, EPP foams are known to be able to absorb kinetic energy without fracturing. Thus, EPP is often used in safety components related to crashworthiness by the automotive industry (e.g. interior crash pads for head/knee protection and bumper cores). EPP is made of pellets produced by a foamed polypropylene. After various pre-treatments, the foam products are created by steam chest moulding of the pellets. Three types of EPP have been applied in this study: EPP-5122, EPP-5130 and EPP-5170 with nominal densities of 30, 50 and 100 kg/m^3, respectively. Here the two last digits in the name indicate the bulk density (in kg/m^3) of the beads. The EPP foam with the lowest density (30 kg/m^3) was delivered as plates cut from a block of material with nominal dimensions 1200 mm × 800 mm × 180 mm, while the two other EPP foams were delivered as plates with nominal dimensions 2000 mm × 1000 mm × 50 mm.

Nominal mechanical properties of both XPS and EPP are provided in Table 1. SEM images of the foams revealed that the microstructure of XPS and EPP in this study is similar, but the cell size seems to be somewhat smaller for the latter [30].

2.2 Material tests and results

Material tests on similar Docol 600DL plates have previously been carried out by e.g. Rakvåg et al. [33] and Holmen et al. [34]. In the quasi-static setup, triplicate tests were performed in three different in-plane directions with respect to the rolling direction of the

plate. The crosshead velocity of the universal test machine was 2.0 mm/min in all tests, giving an initial strain rate of 5×10^{-4} s^{-1} in the gauge area of the specimen. During testing, the force was measured by a load cell, while the displacement of the specimen was measured by both an extensometer and 2D-DIC. The dynamic material tests were carried out in a split-Hopkinson tensile bar (SHTB). Force-elongation curves and true stress-plastic strain curves until necking in different material directions from quasi-static tensile tests on the steel skins used in this study can be found in [30]. These tests revealed that the skin material can be considered isotropic with a small variation in elongation to failure, while the dynamic tensile tests showed that this steel alloy is only moderately strain-rate sensitive.

Uniaxial compression tests of the polymer foams were performed on cubic specimens with edge lengths of 50 mm under displacement control in an Instron universal testing machine. The mechanical response of the different foams were realized through three test series, and all tests were repeated five times. In Series 1, the anisotropy of the foams was revealed by conducting compression tests on cubes loaded in the thickness (normal) direction (ND), the longitudinal direction (LD) and the transverse direction (TD) of the plates. The crosshead velocity of the test machine was 3.0 mm/min in these tests, giving an initial strain rate of 1×10^{-3} s^{-1}. In Series 2, the inherent surface layers due to the production process were removed on some of the foams to check if this affected the overall mechanical response of the material. Also these test were conducted at a strain rate of 1×10^{-3} s^{-1}. In Series 3, the strain-rate sensitivity of the foams was partly explored by rerunning all tests in ND at higher loading rates. The crosshead velocity of the test machine in these tests was increased to 30 mm/min and 300 mm/min, giving strain rates of 1×10^{-2} s^{-1} and 1×10^{-1} s^{-1}, respectively. Although these strain rates are lower than those found in typical impact events, they give an idea about the materials sensitivity to increased loading rates. The complete test matrix for the foam compression tests is given in Table 1.

Prior to testing, each sample was given an identification number before being carefully measured and weighed. The densities were determined from these measurements and they are given in Table 2. During testing, the specimens were compressed between two hardened steel platens. The load was registered with a calibrated load cell, while the displacement was measured both by the stroke of the test machine and edge tracing of the rigid platens using a predefined vector in the DIC-code eCorr v4.0 [35]. Based on these measurements, engineering and true stress-strain curves were established. Note that Poisson's ratio was considered negligible in the calculation of the true stresses. All tests were automatically

stopped when the force reached approximately 5 kN. Pictures for both local and global 2D-DIC analyses were provided, and a fine-graded speckle pattern was applied to the foam samples before testing to get an increased contrast for the displacement- and strain-field measurements.

Experimental results in terms of true stress-strain curves from Series 1 and 2 are presented in [30], but some of the main findings are included in the following for completeness. All samples showed typical closed-cell foam behaviour [9], i.e., a linear elastic region, a plateau region with large deformations, and finally a densification region where the cells become more and more compacted. Table 2 displays the mean values of density ρ, elastic modulus E, yield stress σ_y, plateau stress σ_p and densification strain ε_D for the tests in ND at a strain rate of 1×10^{-3} s^{-1}. Here, E is calculated from the linear elastic region of the stress-strain curve, σ_p is taken as the mean stress in the interval between 0.2 and 0.4 compressive strain, while σ_y and ε_D are obtained by a best fit to a crushable foam model from the literature (see [36] for details).

Some main conclusions were drawn from the quasi-static compression tests. First, the scatter between parallel tests was in general small. Second, the anisotropy of the foams seemed modest, especially for EPP, and that they may be considered isotropic for most engineering applications. Third, the elastic modulus, the yield stress and the plateau stress all display a distinct increase with foam density, which is in accordance with the general behaviour of cellular materials [9]. On the other hand, the densification strain for XPS was rather constant and independent of density, while it decreased with increasing density for EPP. Bear in mind that the density range for the EPP foams is much larger than for the XPS foams considered here. For the same density, XPS foams were found to be significantly stiffer and stronger than corresponding EPP foams (see Table 2). All the tested materials exhibits some strain hardening, leading to a plateau stress that increases with compressive strain. Finally, removing the surface layers of the foam samples did not seem to have any major influence on the global mechanical response of the foams investigated in this study.

True stress-strain curves for XPS and EPP in ND at different strain rates are shown in Figure 1. Since the scatter between parallel tests also in this series was found to be small, only a typical curve is shown. A clear increase in the yield and plateau stress is seen with increasing strain rate, while the effect on the elastic modulus is less distinct. As an example, at a true strain of 0.25 the true stress is increased by roughly 50% when the strain rate is

increased by two decades (i.e., from $1\times10^{-3}\,s^{-1}$ to $1\times10^{-1}\,s^{-1}$) for XPS-400-ND. Another observation from this figure is that while the densification strain for XPS seems to be in the same range, rather independent of density and strain rate, a distinct difference is seen for EPP. Again, one has to keep in mind that the density range of the EPP foams is much larger than for the XPS foams considered. In any case, it seems safe to state that both XPS and EPP are strain-rate sensitive.

When foams are compressed, zones of highly compacted material surrounded by regions with lower strains will form due to the porous structure. As the compression increases, the localised areas extend and propagate outwards [17]. Typical strain fields of both XPS and EPP foams were established using the DIC-code eCorr [35], and can be found in [30] and [37]. These fields revealed a distinct difference in the deformation mode for the two types of foam when crushed, even though the global stress-strain response looks similar. Both foams displayed strain localization with insignificant elongation in the transverse direction, indicating a negligible Poisson's ratio in the plastic domain. However, while the strain localization in XPS was found to start in a sharp band and expand outwards, the strain localization in EPP seemed to appear randomly distributed over the height of the sample. The behaviour was similar for both foam types at elevated strain rates. This local response may explain why EPP foams strain harden more in the plateau region than XPS foams. Since XPS foams are extruded, the density will vary over the thickness, and it is often found to be lower in the centre of the material [38][39]. To examine this for the tested foams, five cubes of each XPS foam density were sliced into five layers of 50 mm × 50 mm × 10 mm, in both ND and LD, before they were weighed and measured. Based on these measurements, the density variation over the thickness and along the length of the plates could be estimated. Figure 2 a) shows the five layers of a sliced cube, while Figure 2 b) displays the estimated density variation over the thickness. The density is significantly lower in the centre of the plate than at the boundaries, especially for XPS-250 and XPS-400. For XPS-700, the density variation over the thickness was lower, but still has a local minimum in the centre. A density variation along LD was also seen, but this was markedly lower than in ND. It is also noteworthy that the strain localization in XPS-700 occurred in bands closer to the surface layers [37] than in the lower density foams where it always took place in the middle [30]. From these results, we conclude that local variations occur between different foam types, even though the global stress-strain response is rather similar. It is also safe to assume a negligible Poisson ratio in the plastic domain for all foams applied.

3. Component tests

3.1 Experimental setups

Both quasi-static and dynamic tests on the different target configurations were carried out to reveal the response during impact loading. The skins were the same in all components, while the core material and density varied. Further, the thickness of the skins and the core was kept constant at 0.8 mm and 50 mm, respectively, whereas the in-plane dimensions were taken as 400 mm × 400 mm in all tests. The different target configurations tested were: 1) sandwich structure, i.e., the target consisted of front and back steel skins with the various polymeric foams described in Section 2 as core, 2) core and back skin, i.e., the target was similar to those in configuration 1, but without the front skin, and 3) skins only, i.e., the target consisted of one or two steel skins without the core. Pictures of the various target configurations in the quasi-static setup are shown in Figure 3, while Figure 4 shows a sketch of the dynamic setup.

In the tests, the square components were bolted to a rigid frame having a circular hole with diameter equal to 300 mm. Clamping was provided by 12 equidistant M12 bolts that fixed the target to the test rig (Figure 3). Each bolt was tightened to 2 Nm using an instrumented torque wrench to avoid damage to the rather soft cores. No clamping ring was used on top of the front skin in any of the tests for the same reason. In all tests, the out-of-plane deflection of the back skin was measured by 3D-DIC. The same frame and impactor nose (Figure 4b) was used in both the quasi-static and dynamic tests. The impactor nose was originally designed to imitate an idealised knee during a crash situation [40], and was therefore found ideal to reveal the energy absorbing capabilities of the various configurations during impact. Prior to testing, the foam cores were measured and weighed to determine the density, and the underside of the back skin facing the cameras was spray-painted with a black and white speckle pattern for the 3D-DIC measurements.

Twenty quasi-static component tests were conducted under displacement control in the same Instron universal testing machine equipped with the same load cell as used in the material tests [30]. In these tests, the loading was stopped at a stroke of 50 mm for the sandwich components, immediately after the first fracture in the foam for the tests without the front skin, or at a force of 95 kN for the skins only. The crosshead velocity during testing was also the same as in the quasi-static material tests, i.e., 3 mm/min. The tests were instrumented

by three Prosilica GC2450 cameras synchronized with the load measurements at a frame rate of 0.5 Hz. Two of the cameras were used to measure the out-of-plane deflection of the back skin by 3D-DIC, while the last camera was applied for point-tracking of the impactor displacement. Camera calibration is required for 3D-DIC in eCorr [35]. This was accomplished by photographing a cylinder covered by a checkerboard pattern with known geometry before and after testing. After calibration, the standard deviation of the error in the calculated 3D model was less than a tenth of a millimetre when compared to the exact geometry (see e.g. [41] for details). Although the quasi-static component tests have been discussed in a previous publication [30], the main results from this study are presented in Section 3.2 for completeness.

Dynamic impact tests were performed on the same target configurations as used in the quasi-static tests at nominal striking velocities v_i of 5, 7 and 10 m/s. In these tests, an Instron CEAST 9350 drop tower, capable of imparting a maximum kinetic energy of 1800 J, was used. The experimental setup is illustrated in Figure 4. In these tests, the standard instrumented striker and striker-holder having masses of 1.435 kg and 4.300 kg, respectively, were used. By including the impactor nose with a mass of 1.660 kg and 7.5 kg additional weights, a total impacting mass m_p of 14.895 kg was achieved. The drop tower permits velocities ranging from 0 to 15.5 m/s for masses of approximately 15 kg [42]. The striker was connected to a calibrated load cell located approximately 220 mm from the tip of the impactor nose. This load cell measured the force at discrete points in time with a temporal resolution of 500 kHz. The measurement duration was 0.04 s for all tests, giving 20,000 data points from each test. The exact striking velocity was measured by a photocell system just prior to impact.

Two synchronised Phantom v1610 high-speed cameras with a resolution of 1280 × 800 pixels and a frame rate of 16,000 frames per second were placed below the target (Figure 4a), and used for 3D-DIC measurements by eCorr [35] to obtain the out-of-plane displacement field of the back skin. From these measurements, the displacement field at the back skin surface as a function of impact force during the experiment was obtained. The accuracy of the dynamic 3D-DIC measurements has been proven in e.g. [41].

Based on the load-cell measurements, the following numerical integration scheme was performed to determine the velocities and displacements from the tests [34]

$$v_{n+1} = v_n - \left(\frac{F_{n+1} + F_n}{2m_p} - g \right) \Delta t, \qquad w_{n+1} = w_n + \left(\frac{v_{n+1} + v_n}{2} \right) \Delta t \tag{1}$$

Here v is the velocity, w is the out-of-plane displacement of the striker, F is the resisting force from the target on the impactor nose, m_p is the total impacting mass, $g = 9.81\,\mathrm{m/s^2}$ is the gravitational acceleration, and Δt is the sampling time. Subscripts $n+1$ and n denote current and previous values, respectively. Since the load cell is not located at the tip of the impactor nose, the mass below the strain gauge must be accounted for in order to find the resisting force from the structure on the impactor. By using dynamic equilibrium, the equation for the resisting force F as a function of the measured force P can be found as [43]

$$F = \left(1 + \frac{m_2}{m_1}\right) P \tag{2}$$

where m_1 is the mass above the load cell, m_2 is the mass below the load cell, and $m_p = m_1 + m_2$ is the total impacting mass. Note that the mass of the striker under the load cell is estimated to 0.492 kg [42]. Thus, with the experimental setup used herein $m_1 = 12.743\,\mathrm{kg}$, $m_2 = 2.152\,\mathrm{kg}$ and $m_2 / m_1 \approx 0.169$. Consequently, the resisting force is 16.9% higher than the measured force.

In total 36 dynamic component tests were carried out using this experimental setup and the main results from the impact tests are presented in Section 3.3. Note that some of the configurations using EPP as core material were not tested with the highest impact velocity due to severe springback of the impactor that potentially could damage the experimental setup.

3.2 Experimental results – quasi-static tests

Experimental data in terms of energy absorption versus stroke displacement from the quasi-static tests can be found in [30] in terms of work W at different levels of striker displacement. Failure in the foam core was not observed in any of the tests for configuration 1, i.e., when the foam core was covered by the front skin. Parallel tests were carried out for some of the configurations, and the scatter was modest. Measured force-displacement curves, displacement profiles of the back skin from 3D-DIC measurements at a stroke of 50 mm, together with pictures of some typical foam cores and skins after testing are also given in [30].

The force level was found, as expected, to increase monotonically with foam density for the same displacement and core material during the quasi-static indentation tests. Furthermore, XPS-700 absorbed the most energy in configuration 1, even though EPP-5170 is more than twice as dense. In general, XPS foams absorbed roughly twice as much energy as EPP foams with similar density at the same displacement. This is related to the higher stiffness and strength of the XPS foams compared to the EPP foams with similar density (Table 2). In configuration 2, however, XPS foams fractured before EPP foams, and EPP-5170 absorbed the most energy at large displacements. This behaviour was further indicated by the measured out-of-plane displacement profiles. These profiles showed that large forces (associated with high energy absorption) resulted in large displacements of the back skin during quasi-static loading. While a foam core of XPS-700 resulted in the largest displacements in configuration 1, EPP-5170 resulted in the largest displacements in configuration 2. Another difference in response between the two foams in configuration 2 was the fracture mode. For XPS the fracture grew almost vertically along the sides of the impactor in a rather brittle manner, while for EPP the fracture developed more diagonally away from the impactor, spreading the applied force over a larger area of the back skin. It was also confirmed that the sandwich structure in configuration 1 absorbed much more energy than the foam cores without the front skin in configuration 2 for the same displacement. This is probably due to membrane stretching of the front skin and a better load distribution over the core at large deformations.

For the skins only, i.e., configuration 3, a complex buckling process took place in the sheets [30], and the load was mainly carried by membrane stretching. The out-of-plane displacement profiles took the form of the impactor, so it was clear that the nose-shape of the impactor affected the results. At a displacement of around 40 mm, the single skin started to fail at the support. Such failure was not observed for the double skins, but the boltholes were clearly elongated. From the 3D-DIC measurements, the calculated strain fields confirmed that the strains in the centre of the back skin were small (typically less than 5%), but much higher (more than 50%) at the boundary. The buckling of the steel sheets around the rim could have been better controlled by a fully clamped boundary, but such boundary conditions are unlikely for this type of energy absorbers. In that sense, the applied boundary conditions are more realistic.

3.3 Experimental results – dynamic tests

The dynamic test results are given in Table 3 in terms of impact velocity (v_i), maximum displacement of the striker (w_m), maximum displacement of the back skin (w_b), maximum resisting force (F_m), impact time (t_i), total impulse (i_t) and total work (W_t). The total impulse and total work were obtained as

$$i_t = \int_0^{t_i} F dt, \qquad W_t = \int_0^{w_m} F dw \tag{3}$$

where F is the resisting force, t is the impact time and w is the displacement of the striker. Figure 5 to Figure 7 provide resistance force-displacement curves from all the component tests, including the quasi-static tests. The quasi-static curves follow as seen the dynamic curves, but a clear dynamic effect in terms of an increased force at the same displacement is in general observed.

From the experimental data one can see that most variables (the maximum displacement of the striker, the maximum resisting force, the total impulse and the total work) increases significantly with impact velocity for all configurations. The exception is the impact time that stays rather constant or reduces with impact velocity. This might be due to an increased elastic rebound with impact velocity, especially for the EPP foams. The maximum resisting force is found in the skins only, i.e., configuration 3, for all impact velocities. Furthermore, the force level is as expected higher and the indentation of the striker lower in configuration 1 than in configuration 2. For low impact velocities, the resisting force is higher in XPS foams than in EPP foams with similar density, but this seems to change as the impact velocity becomes high. This is illustrated in Figure 8, where both the resisting force and the total work is plotted versus impact velocity for configuration 1 and 2. The significant density and strength differences between the materials should, however, be kept in mind. It is also interesting to observe that the energy absorption is somewhat similar for all configurations at constant velocity, and shows an almost linear increase with impact velocity within the limitations of this study. It is thus understood that a low resisting force gives a large striker displacement for the same impact velocity and vice versa, as confirmed by the data in Table 3. However, at the highest impact velocities XPS foams seem to absorb more energy than EPP

foams. The energy absorption is always higher in configuration 2 than in configuration 1 for the XPS foams, but this is not necessarily true for the EPP foams.

Pictures of some typical foam cores after impact are presented in Figure 9 for XPS and in Figure 10 for EPP. The overall conclusion based on visual inspection is that failure did not occur in any of the foam cores when covered by the front skin, i.e., when used in configuration 1. On the other hand, failure always occurred when the front skin was absent, i.e., when used in configuration 2, and more so for the XPS foams. Consequently, failure in the foam core cannot be responsible for the observed difference in force level and energy absorption for the various foams in configuration 1. Figure 10 also shows a picture of the skins only, i.e., configuration 3, after an impact of 10 m/s. Even though much deformed, they are not as damaged as the skins after the quasi-static tests (see [30]). In addition, when the skins are used in combination with a foam core (configuration 1 and 2), they are much less deformed.

Out-of-plane displacement profiles of the back skin at maximum striker indentation based on 3D-DIC measurements for configuration 1 and 2 are shown in Figure 11, while Table 3 provides the maximum displacement w_b. Note that the maximum displacement does not necessarily occur in the centre of the skin. Profiles for configuration 3, i.e., skins only, are not shown for brevity. It is now possible to estimate the foam compression using the data presented in Table 3 by simply subtracting the maximum back-skin displacement w_b from the maximum striker displacement w_m, i.e., $w_c = w_m - w_b$, and the results are plotted in Figure 12.

Figure 11 shows that the structural response is not as intuitive as for the quasi-static tests. For configuration 1 at an impact velocity of 5 m/s, one can e.g. see that the maximum displacement is larger for EPP-5130 than for EPP-5170. Keep in mind that the density is twice as high while the stiffness and strength are three times higher in the latter (see Table 2). This results in a higher energy absorption in EPP-5130, albeit the resisting force is higher in EPP-5170, as shown in Table 3. A similar behaviour is observed for some of the XPS cores. The stiffer XPS cores cause in general larger maximum displacements than the EPP cores, but for configuration 2 at an impact velocity of 7 m/s, the situation is different. Here the lowest density foam, i.e., EPP-5122, results in the largest displacements of the back skin. This may be caused by complete compaction of the low-strength core, which is partly confirmed at an impact velocity of 10 m/s. At this impact velocity also the lowest density XPS foam seems to be more or less fully compacted in configuration 2 (see Figure 12). Further, for low impact

velocities it seems that low-density foams result in minimum back-skin displacement, and more so for the less stiff EPP foams. Note also that the maximum displacement is similar for configuration 1 and 2 for low impact velocities. However, as the impact velocity is increased, the response seems to change. Now the intermediate density foams seem to give the minimum back-skin displacement, probably due to full compaction of the cores. It is also seen that the maximum displacement is much lower in configuration 1 than in configuration 2 at the highest impact velocity. This is probably caused by membrane stretching of the front skin at large deformation. Finally, the maximum displacements based on 3D-DIC measurements for configuration 3, i.e., skins only, were similar to w_m given in Table 3, and these are larger than if foam is used as core material. From this, it seems safe to state that the response of the different crash components also depends on the impact velocity range.

Figure 12 clearly shows that low-density foams become much more compressed than high-density foams, and the most compressed foam core consists of EPP-5122 independent of configuration or impact velocity. At the highest impact velocity in configuration 2, both EPP-5122, XPS-250 and XPS-400 are almost completely compacted, while this is not possible in configuration 1 due to the front skin. This plot indicates that the low-density core is much more activated in the tests than a corresponding high-density core, and may explain the relatively high energy-absorption in the low-strength foams. However, it also implies that if a low-density foam core is fully compacted, the back skin will deform significantly. It should, however, be pointed out that these results are only confirmed within the rather limited experimental range considered in this study.

4. Discussion

When designing an optimal component for energy absorption during a crash situation, at least four different premises are important. These are: 1) low total weight of the component, 2) low force transfer from the component to the underlying structure, 3) high total energy absorption in the component, and 4) low out-of-plane displacement of the back skin. In addition, complete failure of the whole component could obviously be catastrophic and must consequently be avoided, but since none of the configurations investigated in this study failed at critical points, this is not considered in the following. From the data of the impact tests in Table 3, one can see that when the density of the foam increases, the striker displacement, the impact time and the energy absorption decrease, while the resisting force and the impulse increase, for the same impact velocity.

These trends seem valid independent of foam type and target configuration. For increased impact velocity, all of these parameters increase. The only exception is the impact time that is rather constant for all foams except for the lowest density EPP foam where it decreases in configuration 2. Another important parameter is the out-of-plane displacement w_b of the back skin. This value is in the same order of magnitude independent of foam type for the same impact velocity, but it increases as expected with impact velocity even though not to the same extent as the striker indentation. From these results, it seems clear that in order to minimise the weight, transmitted force and back-skin deflection, and at the same time maximise the energy absorption, a low-density foam should be used as core in a crash component. However, it is then important to avoid full compaction of the foam material, and this may occur as the impact energy (i.e., the impactor mass or velocity) increases.

Another interesting study is the comparison between the response of the crash component with and without the front skin. In these tests, the weight of one steel skin is about 1 kg, while the weight of the foam core varies between 0.24 kg and 0.80 kg depending on the density. Thus, the skins represent 70-90% of the total weight of the component. If the front skin is removed or replaced by a lighter material, the total weight of the crash component can be much reduced. From the data in Table 3, it is seen that if the front skin is removed the energy absorption is in general increased, while the resisting force is reduced, which are both beneficial for increased crashworthiness. For low impact velocities, the displacement of the back skin is hardly affected, but for the highest impact velocity, the difference in back-skin deflection between covered and uncovered components becomes large for the weakest foams. This is because the core becomes almost fully compacted at the highest impact velocities when unprotected. However, the striker indentation increases significantly as expected when the crash component is uncovered, and the foam core will fail. Failure in the foam was not observed when the core was covered. In any case, these results indicate that the mechanical response of the front skin is not vital in order to make an efficient crash absorber. As long as the back skin is strong enough to carry the loading, the front skin can be replaced by a weaker and more lightweight material.

It is also of interest to compare the mechanical behaviour of different foams with similar density. Under such conditions, the mass of the crash component will be the same, so the possible difference in response is only due to the core material. Here, XPS-700 and EPP-5130 have practically identical densities, while the density of XPS-250 is approximately 10%

higher than that of EPP-5122. Keep in mind that the stiffness and strength of the XPS foams are significantly higher than for the corresponding EPP foams (see e.g. Table 2). From Table 3 it is seen that in terms of energy absorption, the difference between XPS-700 and EPP-5130 is minor. However, the resisting force and the back-skin displacement is lower, while the stroke indentation is higher for EPP-5130 than for XPS-700. If we compare XPS-250 and EPP-5122, it is seen that the energy absorption in XPS-250 is in general higher than for EPP-5122, but this can probably be explained by the 10% difference in density between the foams. Even though it is hard to make strict conclusions based on a limited number of tests, these results indicate that the core material itself is of second-order importance compared to the density of the foam.

It is customary to characterise the efficiency of energy absorbers in terms of their specific work W_s [44]. This is in the following defined as the total work W_t absorbed by the component divided by its total weight m_t, i.e.,

$$W_s = \frac{W_t}{m_t} \tag{4}$$

In this study, m_t varies from a minimum of 1.24 kg using EPP-5122 in configuration 2 to a maximum of 2.80 kg using EPP-5170 in configuration 1, while W_t from the impact tests are given in Table 3. A comparison of W_s for the investigated components versus impact velocity is given in Figure 13. It is seen that the overall response is somewhat different from the one based on the absolute values given in Figure 8. The major distinction is that the beneficial behaviour of the components with a low-density core both in configuration 1 and especially in configuration 2 becomes clearer. While the total work during impact is about the same for the different foams in configuration 1 and 2, it is seen that the specific work for a component in configuration 2 is roughly twice as high as in configuration 1 for the same foam core and impact velocity. The figure also indicates that XPS foams are slightly more efficient than EPP foams in both configurations, but due to the lack of data for EPP foams at the highest impact velocities it is difficult to conclude based on this. Note also that according to Figure 13, configuration 3 (i.e., skins only without a foam core) seems to be a very efficient energy absorber, but for this component both the resisting force (Figure 8) and the back-skin displacement (Table 3) becomes unacceptably high as the impact velocity increases.

As an alternative, Mohotti et al. [45] introduced an energy efficiency parameter E_d for low velocity impacts. This parameter allows us to compare results in terms of energy absorption per unit maximum back-skin displacement. Here, E_d is given as the total kinetic energy $K_t = \frac{1}{2} m_p v_i^2$ of the impactor divided by the maximum deformation of the back skin w_b, i.e.,

$$E_d = \frac{K_t}{w_b} \tag{5}$$

where $m_p = 14.895$ kg in this study and the other variables are given in Table 3. Note that according to the work-energy theorem we have that $W_t = \Delta K_t$, and not all of the kinetic energy in these tests is converted into work due to the springback of the impactor. Calculated E_d for the investigated components versus impact velocity are also provided in Figure 13. The results are somewhat different from those obtained using the specific energies. Now it seems like the intermediate-density foams have the highest energy efficiency, especially when the velocity increases, while the low-density foams are still the most efficient at low impact velocities. This was also confirmed by the displacement profiles in Figure 11. Further, EPP foams seem to be more efficient than XPS foams, but the differences are minor. It is also seen that configuration 3, i.e., skins only, is not so attractive anymore. From this, it may be concluded that there is a competition between the various responses. Within the experimental limitations in this study, the general trend is that a crash component with a low-density foam behaves best as long as the impact velocity is low. However, this seems to change as the velocity is increased, especially if the out-of-plane displacement of the back skin is important. For such situations, an intermediate-density foam, that prevents complete compaction of the core of the crash component, seems to be a more efficient energy absorber.

It is difficult to make strict conclusions based on the results presented above, but it seems apparent that the maximum displacement of the back skin, the resisting force and the energy absorption depends on both the core material and the velocity range. At low impact velocities, a low-density foam core seems to give the most efficient crash component, but this may change as the impact velocity is increased. Consequently, it is not obvious which combination of the variables that gives the best energy absorption, but it should be possible to find an optimized combination of the component mass, force level, energy absorption and displacement of the back skin by proper design within a given impact velocity range.

However, such an optimization requires numerical simulations, which is outside the scope of this study. It is also important to state that the obtained data are sensitive to the shape of the impactor nose, and that the results presented herein are only valid within the experimental limitations given.

5. Conclusions

In this study, we have experimentally investigated the energy absorbing capability of two different polymeric foams (XPS and EPP) with varying density used as core material in a crash component. In addition to a number of material tests, both quasi-static and dynamic impact tests have been performed on three different target configurations. The following main conclusions can be drawn based on the obtained results:

- From the 180 compression tests on square foam samples, the scatter between parallel tests was found to be small. Some anisotropy between different loading directions has been observed, but the foams may be considered isotropic for most engineering applications. As expected, the elastic modulus, the yield stress and the plateau stress increased significantly with foam density, while the inherent surface layers on the various foams did not affect the overall mechanical response of the materials very much. However, XPS foams were found to be much stiffer and stronger than EPP foams with corresponding density. Both foam types revealed viscoelastic behaviour and strong strain-rate sensitivity at elevated strain rate. Finally, based on DIC measurements the strain localization was found to be very different between the foam types even though the global mechanical response was similar. This could be attributed to the density variation through the thickness in XPS foams.
- From the 20 quasi-static impact tests, it was observed that the force level and energy absorption increased as expected monotonically with foam density both for the covered and uncovered components. It was also established that the XPS foams absorbed approximately twice as much energy as the EPP foams with the same density at the same displacement. When the foams were unprotected, they failed in some shear fracture mode, and the rather brittle XPS foams failed before the EPP foams. For the skins only, a rather complex buckling mode took place. At large displacements, the force increased rapidly, indicating that the loading was carried by membrane stretching in the metal skins.

- From the 36 dynamic impact tests, the main finding was that in order to minimise the weight, transmitted force and back-skin deflection, and at the same time maximise the energy absorption, a low-density foam should be used as core material in the crash component. It was also found that the response of the front skin is not essential in order to make an efficient energy absorber. Thus, the weight of the crash component can be significantly reduced by using a lightweight and less strong material as front skin. By comparing the mechanical behaviour of XPS and EPP foams with similar density, it was found that the core material itself is of second-order importance compared to the density of the foam. This is contradictory to the observations in the quasi-static tests, where the energy absorption depended on the core material.
- Within the experimental limitations of this study, the general trend is that a crash component with a low-density foam is superior as long as the impact velocity is low, but this seems to change as the velocity is increased due to compaction of the core. For such situations, an intermediate-density foam that prevents such compaction seems to be more efficient. Consequently, it is not obvious which combination of the different variables that gives the best energy absorption.

A natural continuation of the presented research is to use the experimental data presented herein to calibrate and validate numerical models for finite element simulations of the crash components during impact loading. To do so, efficient and accurate numerical algorithms and models for the polymeric foams including both strain-rate sensitivity and fracture are required. It would then be possible to maximise the energy absorption in the crash component, and at the same time minimise the weight, the transmitted force and the back skin displacement, by an optimization tool. That is left for future studies.

Acknowledgement

The present work has been carried out with financial support from Centre of Advanced Structural Analysis (CASA), Centre for Research-based Innovation, at the Norwegian University of Science and Technology (NTNU) and the Research Council of Norway through project no. 237885 (CASA). The authors would like to acknowledge Dr. Egil Fagerholt, Mr. Trond Auestad, Mr. Bjarki Sigurdsson, Mr. Asle Tomstad, Mr. Sindre Berdal, and Mr. Lars Einar Bjørgo for assistance with the various experimental programs.

References

[1] Paulino M, Teixeira-Dias F. An energy absorption performance index for cellular materials – development of a side-impact cork padding. International Journal of Crashworthiness 2011;16:135-153.

[2] Wang D, Zhang S, Wang C, Zhang C. Structure-material-performance integration lightweight optimisation design for frontal bumper system. International Journal of Crashworthiness 2018;23:311-327.

[3] Avalle M, Belingardi G, Ibba A. Mechanical models of cellular solids: Parameters identification from experimental tests. International Journal of Impact Engineering 2007;34:3-27.

[4] Aluminium Automotive Manual: Crash management systems. Retrieved from https://european-aluminium.eu/resource-hub/aluminium-automotive-manual/ [cited: 03.05.19].

[5] Karagiozova D, Langdon GS, Nurick GN. Blast attenuation in Cymat foam core sacrificial claddings. International Journal of Mechanical Sciences 2010;52:758-776.

[6] Avalle M, Belingardi G, Montanini R. Characterization of polymeric structural foams under compressive impact loading by means of energy-absorption diagram. International Journal of Impact Engineering 2001;25:455-472.

[7] Cui L, Kiernan S, Gilchrist MD. Designing the energy absorption capacity of functionally graded foam materials. Materials Science and Engineering: A 2009;507:215-225.

[8] Ryan S, Hedman T, Christiansen EL. Honeycomb vs. foam: Evaluating potential upgrades to ISS module shielding. Acta Astronautica 2010;67:818-825.

[9] Gibson LJ, Ashby MF. Cellular solids: Structure and properties. Second edition, 1997.

[10] Cronin DS, Ouellet S. Low density polyethylene, expanded polystyrene and expanded polypropylene: Strain rate and size effects on mechanical properties. Polymer Testing 2016;53:40-50.

[11] Li QM, Magkiriadis I, Harrigan JJ. Compressive strain at the onset of densification of cellular solids. Journal of Cellular Plastics 2006;42:371-392.

[12] Bouix R, Viot P, Lataillade JL. Polypropylene foam behaviour under dynamic loadings: Strain rate, density and microstructure effects. International Journal of Impact Engineering 2009;36:329-342.

[13] Zhang J, Kikuchi N, Li V, Yee A, Nusholtz G. Constitutive modeling of polymeric foam material subjected to dynamic crash loading. International Journal of Impact Engineering 1998;21:369-386.

[14] Sun Y, Li QM. Dynamic compressive behaviour of cellular materials: A review of phenomenon, mechanism and modelling. International Journal of Impact Engineering 2018;112:74-115.

[15] Li P, Guo YB, Shim VPW. A constitutive model for transverse isotropic material with anisotropic hardening. International Journal of Solids and Structures 2018;138:40-49.

[16] Marvi-Mashhadi M, Lopes CS, LLorca J. Effect of anisotropy on the mechanical properties of polyurethane foams: An experimental and numerical study. Mechanics of Materials 2018;124:143-154.

[17] Mills N. Polymer Foams Handbook. Oxford, Butterworth-Heinemann, 2007.

[18] Yuen SCK, Nurick GN, Theobald MD, Langdon GS. Sandwich panels subjected to blast loading. In: Shukla A et al. (eds.), Dynamic Failure of Materials and Structures, 297-325, 2010, Springer.

[19] Avachat S, Zhou M. Compressive response of sandwich plates to water-based impulsive loading. International Journal of Impact Engineering 2016;93:196-210.

[20] Ye N, Zhang W, Li D, Huang W, Xie W, Huang X, Jiang X. Dynamic response and failure of sandwich plates with PVC foam core subjected to impulsive loading. International Journal of Impact Engineering 2017;109:121-130.

[21] Chen W, Hao H, Chen S, Hernandez F. Performance of composite structural insulated panel with metal skin subjected to blast loading. Materials and Design 2015;84:194-203.

[22] Karen I, Yazici M, Shukla A. Designing foam filled sandwich panels for blast mitigation using a hybrid evolutionary optimization algorithm. Composite Structures 2016;158:72-82.

[23] Correia JR, Garrido M, Gonilha JA, Branco FA, Reis LG. GFRP sandwich panels with PU foam and PP honeycomb cores for civil engineering structural applications: Effects of introducing strengthening ribs. International Journal of Structural Integrity 2012;3:127-147.

[24] Zhang Y, Zong Z, Liu Q, Ma J, Wu Y, Li Q. Static and dynamic crushing responses of CFRP sandwich panels filled with different reinforced materials. Materials and Design 2017;117:396-408.

[25] Hassan MZ, Cantwell WJ. The influence of core properties on the perforation resistance of sandwich structures - An experimental study. Composites Part B: Engineering 2012;43:3231-3238.

[26] Nasirzadeh R, Sabet AR. Study of foam density variations in composite sandwich panels under high velocity impact loading. International Journal of Impact Engineering 2014;63:129-139.

[27] Maheo L, Viot P. Impact on multi-layered polypropylene foams. International Journal of Impact Engineering 2013;53:84-93.

[28] Koohbor B, Kidane A. Design optimization of continuously and discretely graded foam materials for efficient energy absorption. Materials and Design 2016;102:151-161.

[29] Kelly M, Arora H, Worley A, Kaye M, Linz PD, Hooper PA, Dear JP. Sandwich panel cores for blast applications: Materials and graded density. Experimental Mechanics 2016;56:523-544.

[30] Reyes A, Børvik T. Quasi-static behaviour of crash components with steel skins and polymer foam cores. Materials Today Communications 2018;17:541-553.

[31] http://www.sundegroup.com/ [Cited: 03.05.19].

[32] http://www.arpro.com/ [Cited: 03.05.19].

[33] Rakvåg KG, Underwood NJ, Schleyer GK, Børvik T, Hopperstad OS. Transient pressure loading of clamped metallic plates with pre-formed holes. International Journal of Impact Engineering 2013;53:44-55.

[34] Holmen JK, Hopperstad OS, Børvik, T. Low-velocity impact on multi-layered dual-phase steel plates. International Journal of Impact Engineering 2015;78:161-177.

[35] https://www.ntnu.edu/kt/ecorr [Cited: 03.05.19]

[36] Reyes A, Hopperstad OS, Berstad T, Hanssen AG, Langseth M. Constitutive modeling of aluminum foam including fracture and statistical variation of density. European Journal of Mechanics – A/Solids 2003;22:815-835.

[37] Reyes A, Børvik T. Polymer foam crash components subjected to low velocity impact. Proceedings of the 2nd International Conference on Impact Loading of Structures and Materials (ICILSM2018), May 7-11, 2018, Xi'an, China.

[38] Hegdal JP, Tofteberg TR, Schjelderup T, Hinrichsen EL, Grytten F, Echtermeyer A. Thermal conductivity of anisotropic, inhomogeneous high-density foam calculated from three-dimensional reconstruction of microtome images. Journal of Applied Polymer Science 2013;130:1020-1028.

[39] Vestrum O, Kristoffersen M, Polanco-Loria M, Ilstad H, Langseth M, Børvik T. Quasi-static and dynamic indentation of offshore pipelines with and without multi-layer polymeric coating. Marine Structures 2018;62:60-76.

[40] Berntsen JF. Impact loading on parts made of injection-moulded PP. Master's Thesis, Department of Structural Engineering, Norwegian University of Science and Technology, 2015.

[41] Aune V, Fagerholt E, Langseth M, Børvik T. A shock tube facility to generate blast loading on structures. International Journal of Protective Structures 2016;7:340-366.

[42] http://www.instron.se/sv-se/products/testing-systems/impact-systems/drop-weight-testers/9350-drop-tower [Cited: 03.05.19].

[43] Holmen JK, Olovsson L, Børvik T. Discrete modeling of low-velocity penetration in sand. Computers and Geotechnics 2017;86:21-32.

[44] Jones N. Structural Impact, Cambridge University Press, UK, 1999.

[45] Mohotti D, Ngo T, Raman SN, Ali M, Mendis P. Plastic deformation of polyurea coated composite aluminium plates subjected to low velocity impact. Materials and Design 2014;56:696-713.

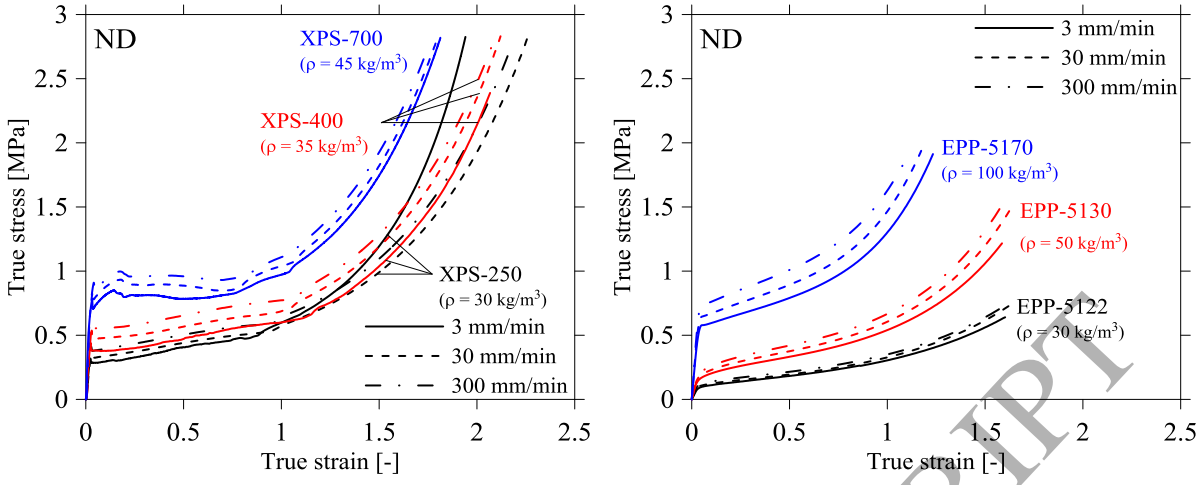

Figure 1. Typical true stress-strain curves from material compression tests of XPS (left) and EPP (right) foams in ND as function of density and strain rate.

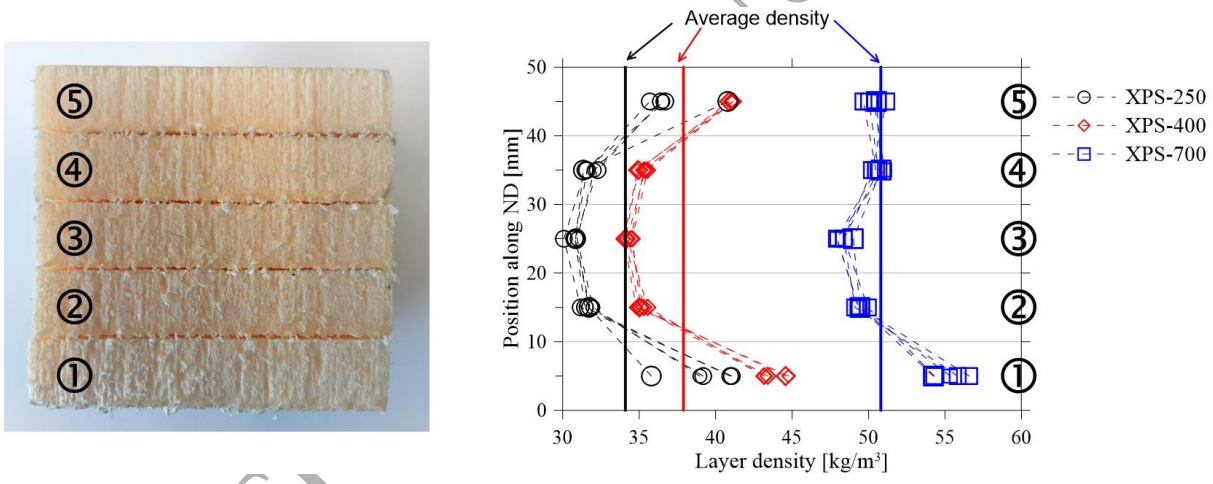

a) b)

Figure 2. a) Foam specimen divided into five layers and b) density variation through the thickness (ND) of the different XPS foams.

a) b) c)

Figure 3. Pictures of the target configurations used in the different test setups [30]: a) Sandwich structure with foam core (here EPP-5170) and front and back skins in Docol 600 DL, b) component with foam core (here XPS-250) without the front skin, but with back skin in Docol 600DL and c) only skins in Docol 600DL without the foam core.

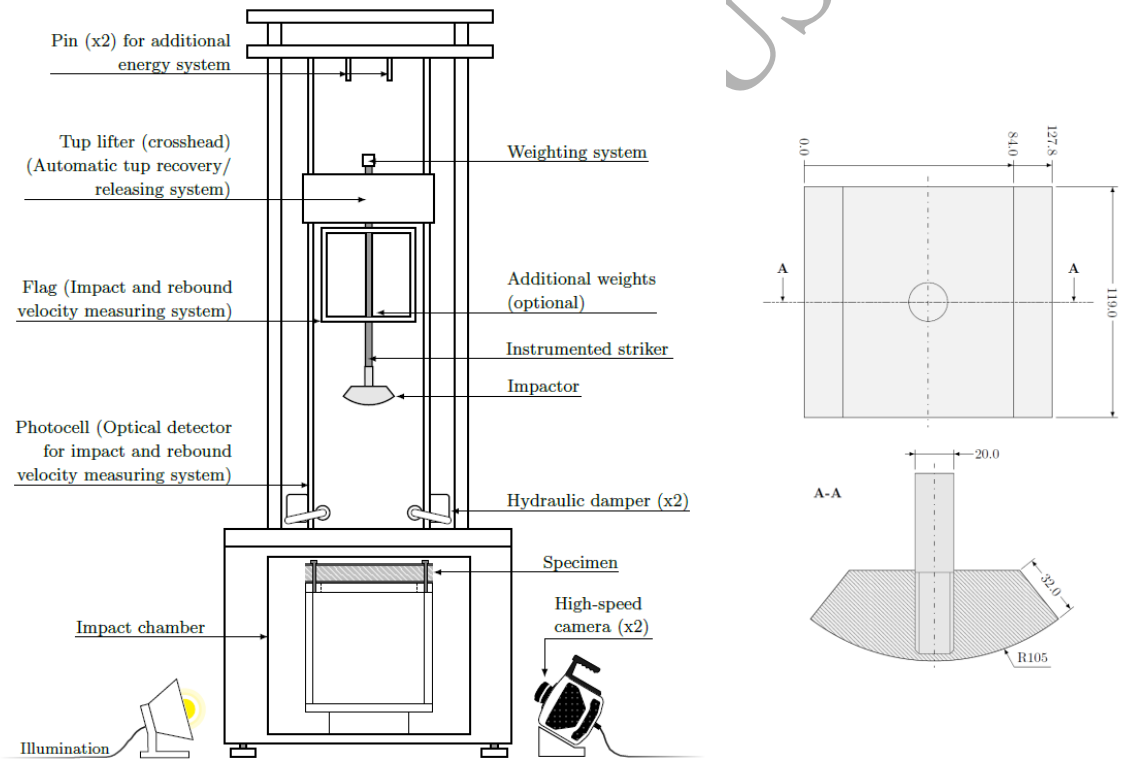

a) b)

Figure 4. Experimental setup for the impact tests: a) drop tower and b) impactor nose.

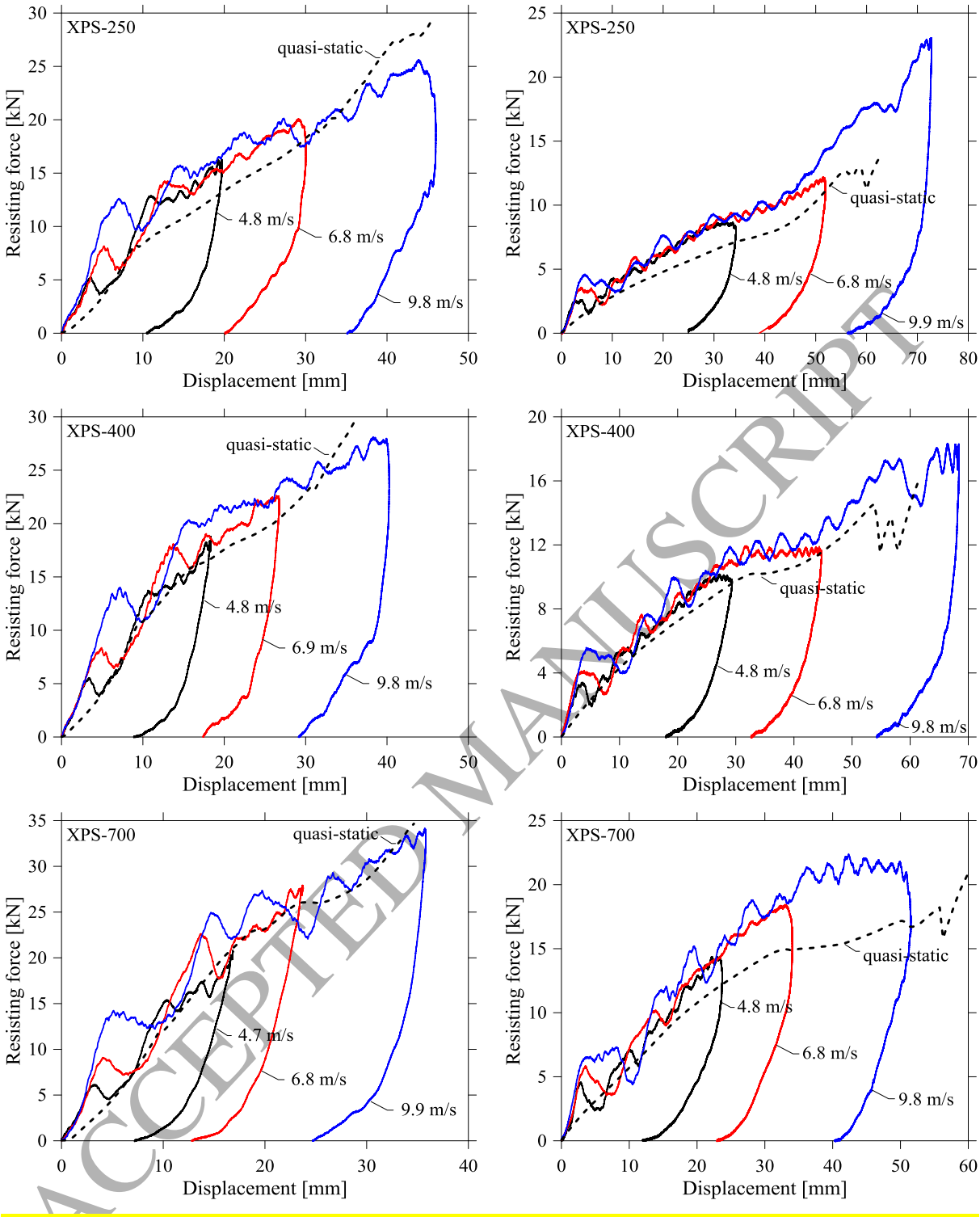

Figure 5. Measured data from quasi-static and impact tests on configuration 1 (left) and configuration 2 (right) with XPS foam cores.

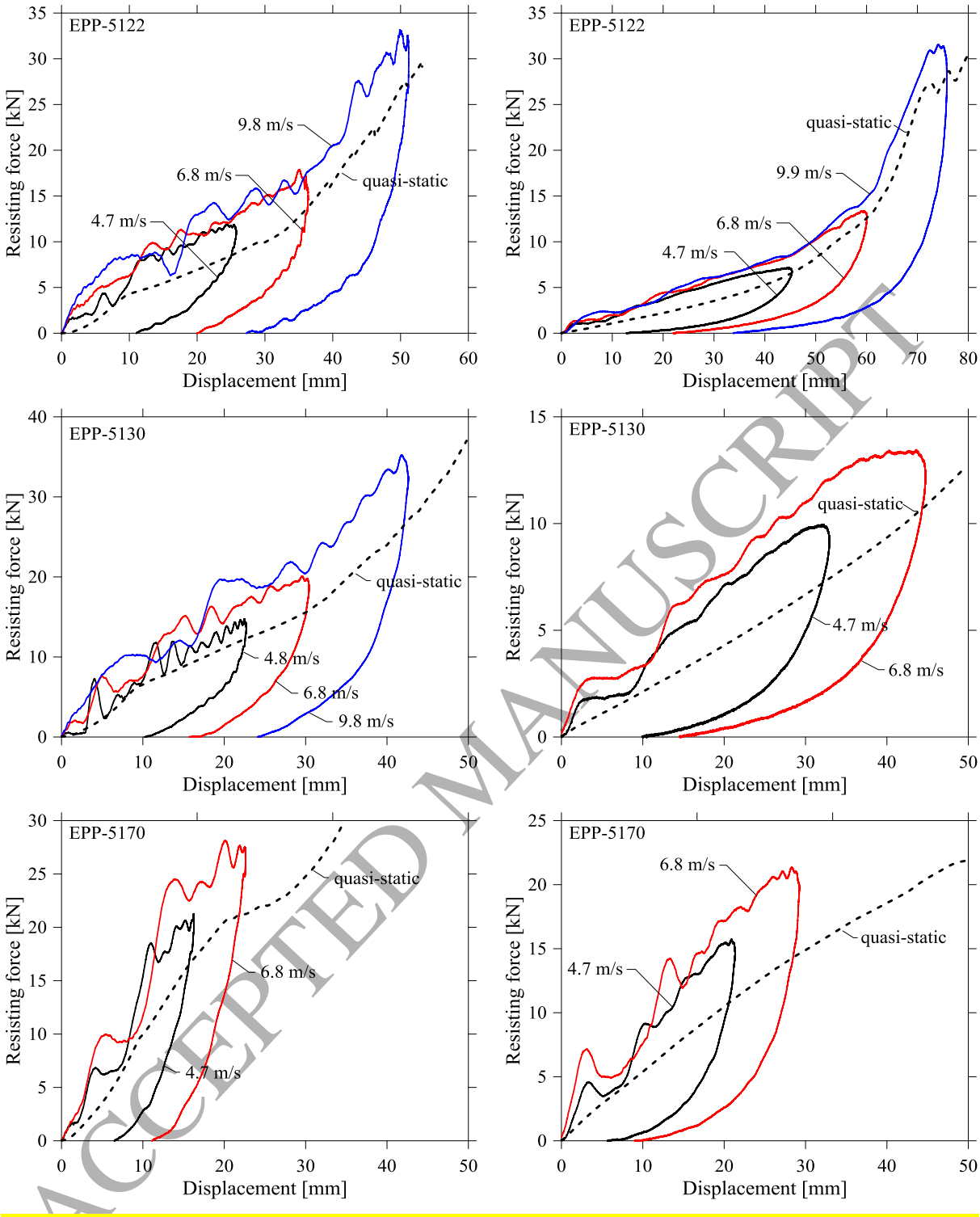

Figure 6. Measured data from quasi-static and impact tests on configuration 1 (left) and configuration 2 (right) with EPP foam cores.

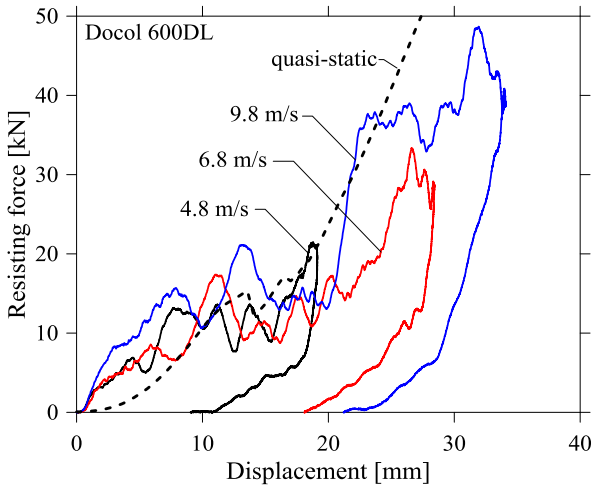

Figure 7. Measured data from quasi-static and impact tests on configuration 3.

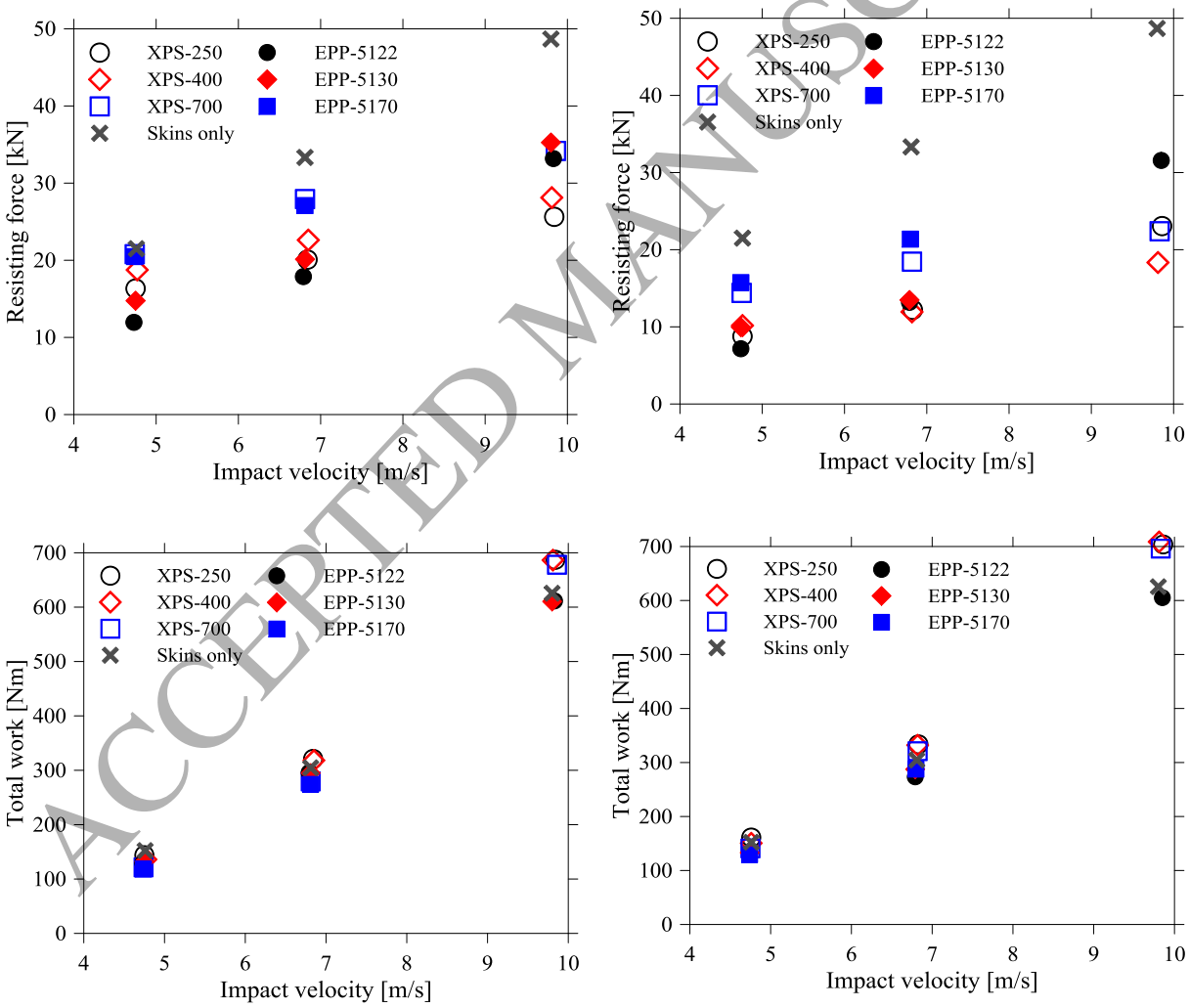

a) With front skin b) Without front skin

Figure 8. Resisting force and total work versus impact velocity for a) configuration 1 and b) configuration 2. The results from configuration 3 are included for comparison.

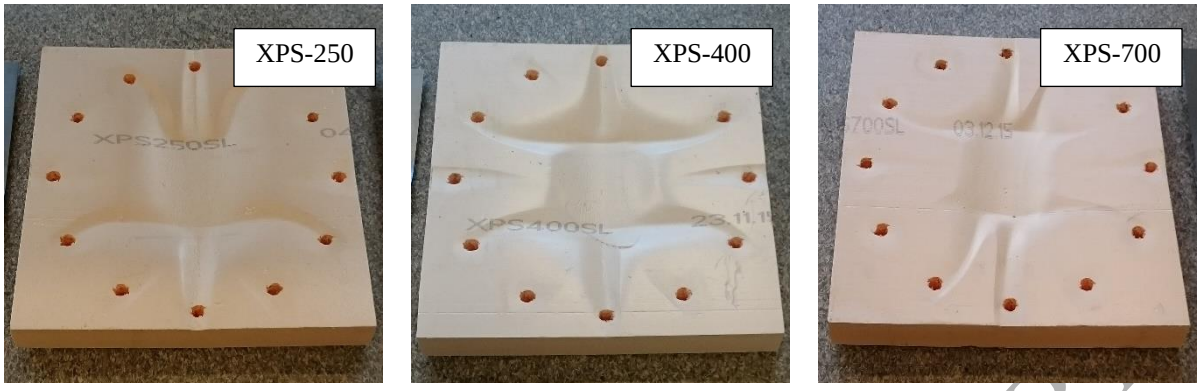

a) With front skin

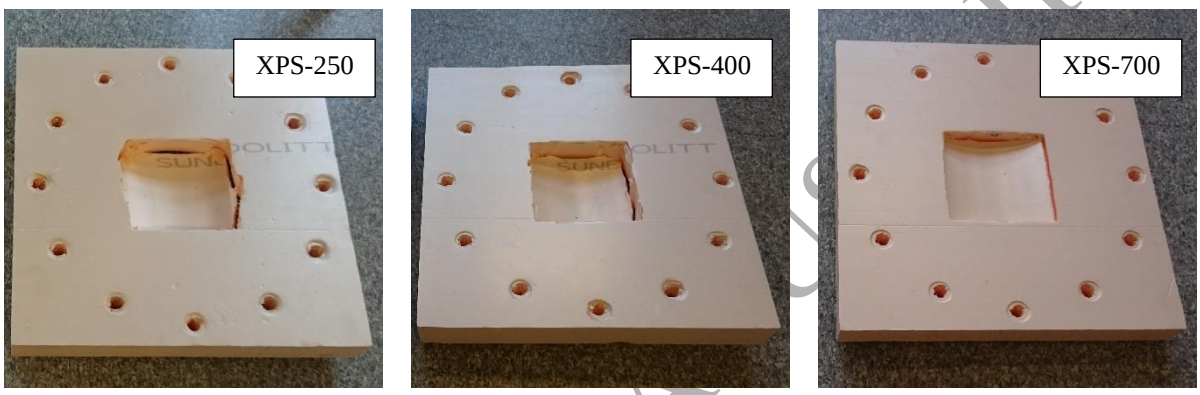

b) Without front skin

Figure 9. Pictures of typical XPS foam cores from a) configuration 1 and b) configuration 2 after an impact of 10 m/s.

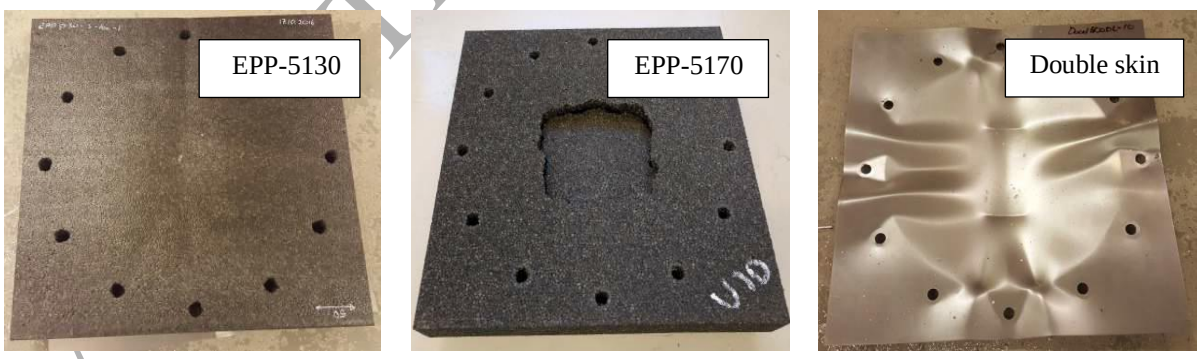

a) With front skin b) Without front skin c) Skins only

Figure 10. Pictures of typical EPP foam cores from a) configuration 1 and b) configuration 2, and c) picture of configuration 3, after an impact of 10 m/s.

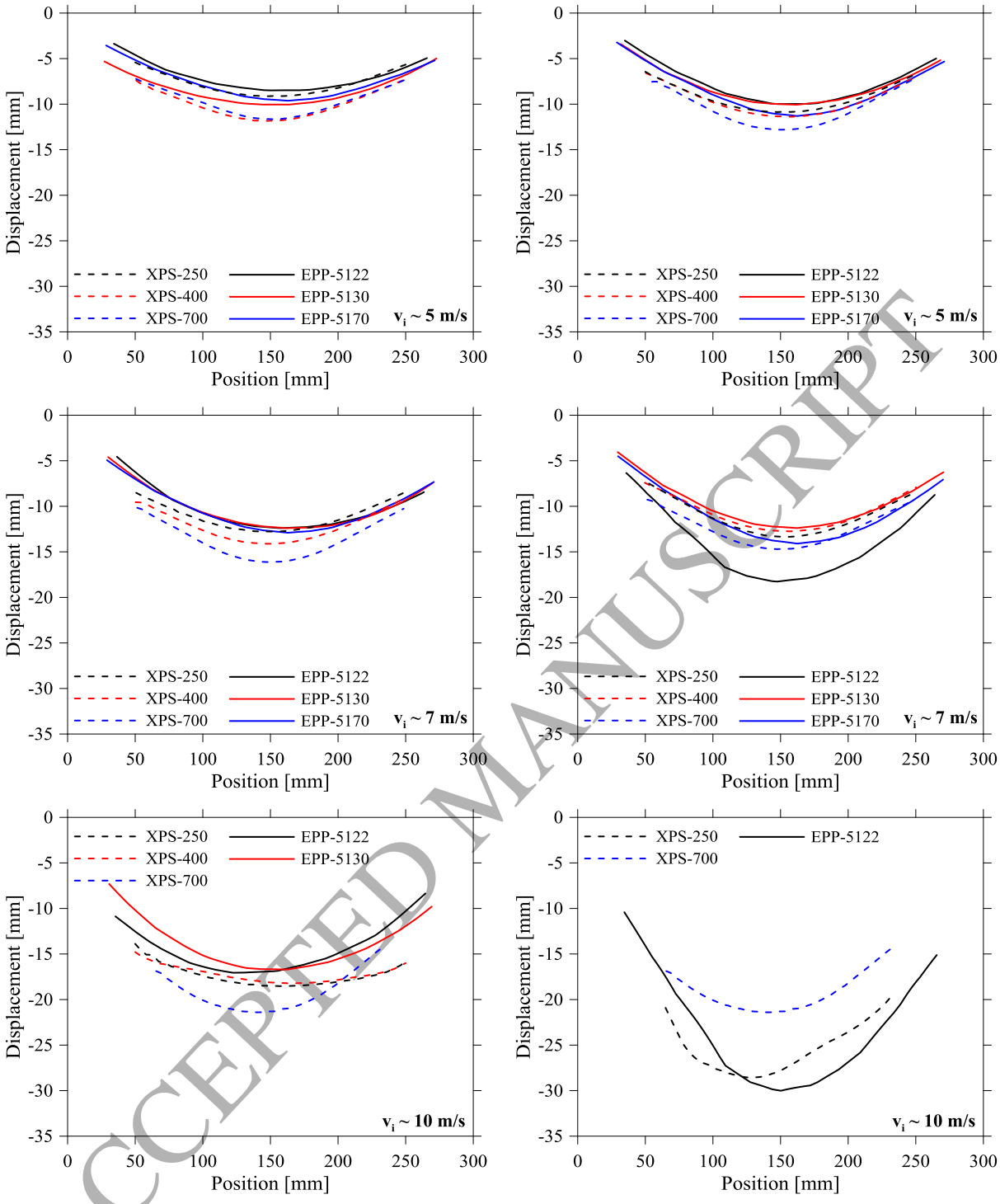

a) With front skin

b) Without front skin

Figure 11. Displacement profiles for the dynamic tests, at maximum displacement of the back sheet from 3D-DIC measurements at various velocities for a) configuration 1 and b) configuration 2.

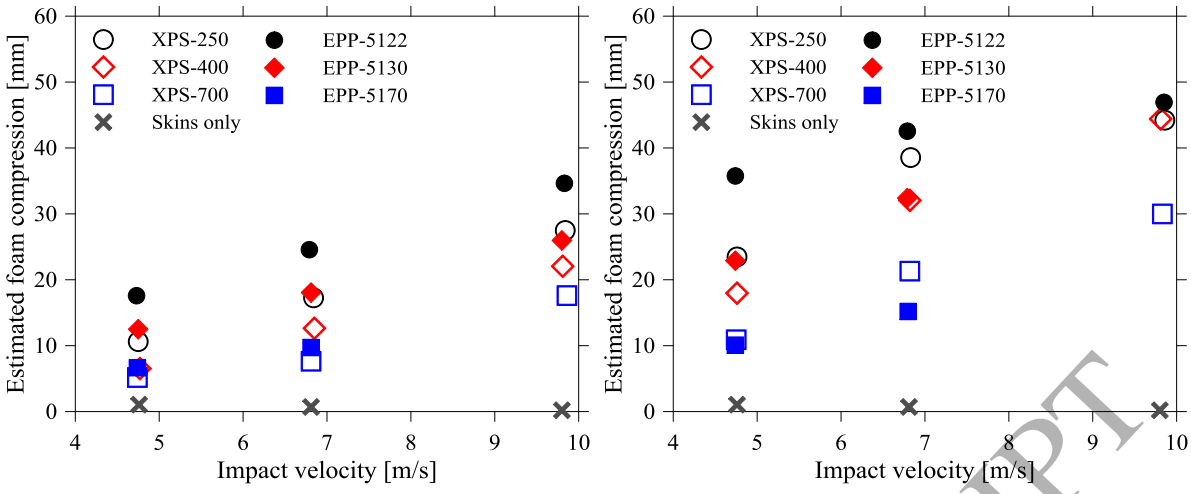

a) With front skin

b) Without front skin

Figure 12. Estimated compression of foam for a) configuration 1 and b) configuration 2. The results from configuration 3 are included for comparison.

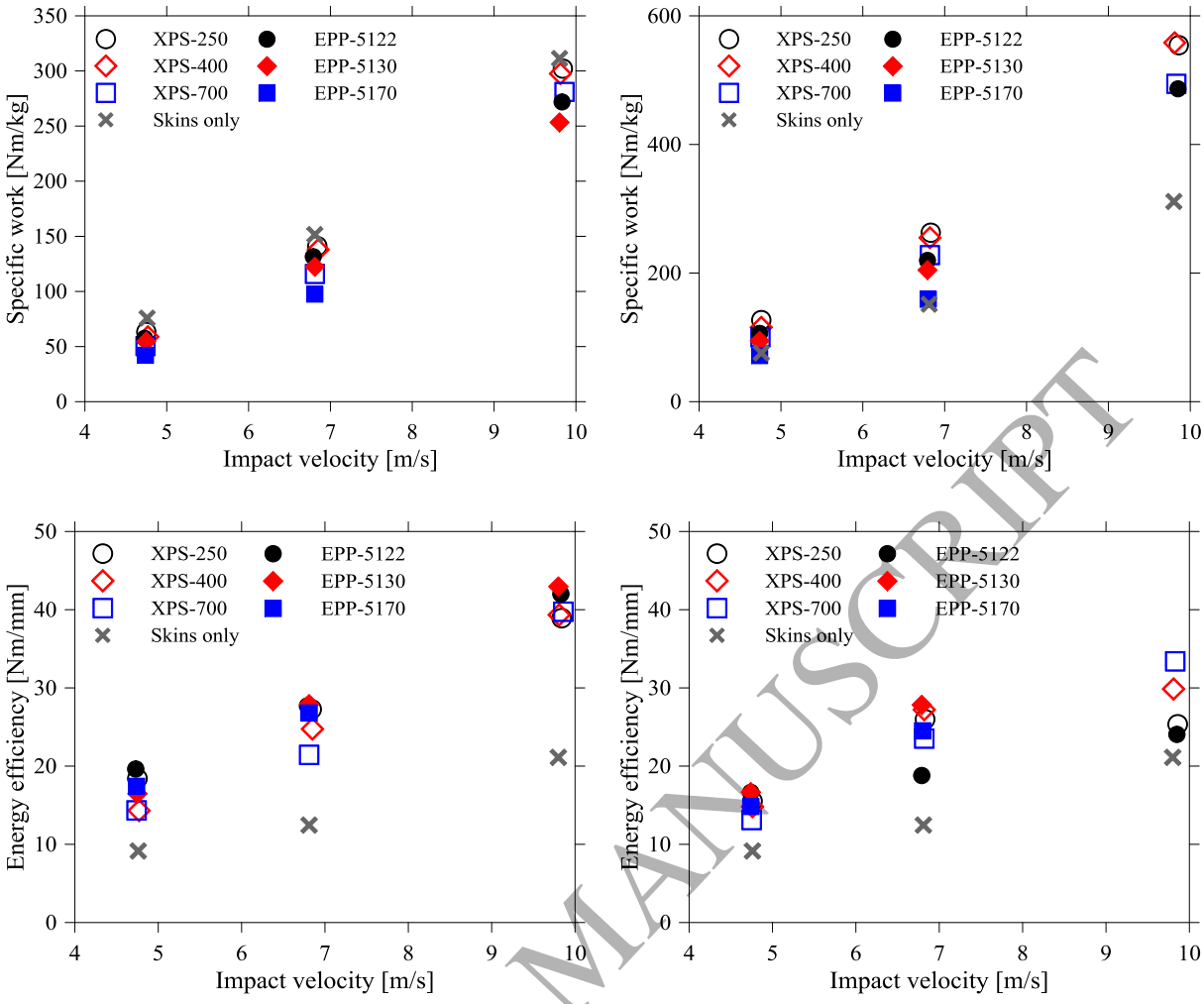

a) With front skin b) Without front skin

Figure 13. Specific work and energy efficiency for a) configuration 1 and b) configuration 2. The results from configuration 3 are included for comparison.

Table 1. Nominal material properties and test matrix for material tests.

Material	Name	Nominal properties			Direction	Test matrix (# of samples)			
						Strain rate [s^{-1}]			
						10^{-3}		10^{-2}	10^{-1}
		Density ρ [kg/mm^3]	Elastic modulus E [MPa]	Compressive strength σ_c^* [MPa]		Surface layer			
						with	w/o	with	with
Extruded polystyrene	XPS-250	30	9.0	0.25	ND	5	-	5	5
					LD	5	-	-	-
					TD	5	-	-	-
	XPS-400	35	15.3	0.40	ND	5	5	5	5
					LD	5	5	-	-
					TD	5	5	-	-
	XPS-700	45	31.0	0.70	ND	5	-	5	5
					LD	5	-	-	-
					TD	5	-	-	-
Expanded polypropylene	EPP-5122	30	2.5	0.15	ND	5	-	5	5
					LD	5	-	-	-
					TD	5	-	-	-
	EPP-5130	50	5.1	0.28	ND	5	-	5	5
					LD	5	-	-	-
					TD	5	-	-	-
	EPP-5170	100	14.3	0.70	ND	5	5	5	5
					LD	5	5	-	-
					TD	5	5	-	-

* At 10% strain for XPS and 25% strain for EPP.

Table 2. Properties (mean values) of foam samples in ND [30].

Material	Density ρ [kg/mm^3]		Elastic modulus E [MPa]	Yield stress σ_y [MPa]	Plateau stress σ_p [MPa]	Densification strain ε_D [-]
	Mean	SD				
XPS-250	34.1	0.38	13.7	0.26	0.34	3.36
XPS-400	37.9	0.65	18.5	0.41	0.49	3.68
XPS-700	50.8	0.38	23.5	0.73	0.77	3.46
EPP-5122	29.9	0.52	3.3	0.10	0.16	3.69
EPP-5130	50.7	0.73	5.9	0.19	0.29	2.97
EPP-5170	102.5	1.47	14.5	0.56	0.72	2.65

Table 3. Impact data from component tests.

Material	Front skin	Measured core height h_{ct} [mm]	Measured density ρ_f [kg/m^3]	Impact velocity v_i [m/s]	Max striker displacement w_m [mm]	Max displacement of back skin w_b [mm]	Max resisting force F_m [kN]	Impact time t_i [ms]	Total impulse i_t [Ns]	Total work W_t [Nm]
XPS-250	Yes	50.8	33.1	4.75	19.74	9.13	16.33	12.60	108.8	143.8
	No	50.8	33.1	4.76	34.34	10.87	8.77	21.07	102.6	161.1
	Yes	50.9	33.1	6.84	30.03	12.78	20.08	13.11	146.5	320.9
	No	50.8	33.2	6.83	51.91	13.37	12.21	21.13	142.9	333.6
	Yes	50.7	33.1	9.84	46.01	18.53	25.63	13.55	201.9	687.1
	No	50.8	33.1	9.86	72.78	28.57	23.06	19.06	199.6	703.8
XPS-400	Yes	52.9	37.2	4.77	18.36	11.84	18.75	11.46	112.8	136.0
	No	52.7	37.5	4.76	29.36	11.39	10.17	18.11	107.3	150.6
	Yes	52.8	37.3	6.85	26.76	14.12	22.62	11.49	147.6	318.2
	No	52.8	37.2	6.82	44.77	12.73	11.94	19.05	142.0	332.1
	Yes	52.8	37.3	9.81	40.27	18.22	28.12	12.50	199.4	686.5
	No	52.8	37.2	9.81	68.41	24*	18.34	19.33	193.8	708.7
XPS-700	Yes	50.2	50.4	4.74	16.84	11.67	20.79	10.53	117.1	121.5
	No	50.2	50.4	4.75	23.72	12.82	14.40	15.18	110.8	140.9
	Yes	50.1	50.4	6.81	23.75	16.11	27.93	10.12	158.4	279.5
	No	50.5	50.2	6.82	34.04	14.73	18.45	14.58	145.9	320.9
	Yes	50.4	50.3	9.86	35.82	21.40	34.17	10.70	205.2	678.0
	No	50.4	50.4	9.83	51.54	21.55	22.39	14.75	198.9	696.0
EPP-5122	Yes	49.9	29.9	4.73	25.77	8.49	11.95	17.27	114.7	129.2
	No	50.0	27.9	4.74	45.32	10.06	7.16	32.88	116.6	132.1
	Yes	49.7	29.5	6.79	36.37	12.40	17.88	16.76	153.5	295.8
	No	49.8	29.8	6.79	60.08	18.27	13.39	28.09	162.6	273.3
	Yes	49.7	30.3	9.83	51.20	17.13	33.18	15.41	221.9	611.4
	No	49.7	30.2	9.85	75.78	30.04	31.57	22.47	225.7	605.2
EPP-5130	Yes	48.7	49.6	4.75	22.70	10.20	14.76	14.79	114.7	131.8
	No	49.4	49.0	4.74	32.94	10.04	9.97	23.59	115.0	133.0
	Yes	48.1	49.0	6.81	30.43	12.37	20.13	14.09	154.4	295.0
	No	49.6	49.1	6.79	44.73	12.34	13.48	23.60	157.3	287.5
	Yes	48.5	48.9	9.80	42.62	16.65	35.26	12.81	220.2	610.5
EPP-5170	Yes	49.5	99.2	4.74	16.27	9.61	21.28	10.31	118.3	118.3
	No	47.7	101.7	4.74	21.35	11.27	15.74	15.32	115.1	129.3
	Yes	49.5	101.0	6.81	22.61	12.89	28.15	10.07	160.1	274.2
	No	49.5	101.9	6.80	29.24	14.05	21.37	15.46	156.2	287.6
Double skin	Yes	2×0.8	7850	4.76	19.12	18.45	21.50	12.59	110.8	152.3
	Yes	2×0.8	7850	6.81	28.42	27.72	33.33	11.20	154.8	304.6
	Yes	2×0.8	7850	9.80	34.07	33.87	48.68	9.61	218.8	625.6

* This result was estimated after the test due to the lack of reliable 3D-DIC data.